Modeling and efficient computation of nonlinear radiation trapping in three-level atomic vapors

A. F. Molisch, W. Schupita, B. P. Oehry, B. Sumetsberger, and G. Magerl
Institut für Nachrichtentechnik und Hochfrequenztechnik, Technische Universität Wien, Gußhausstraße 25/389, A-1040 Vienna, Austria
(Received 9 November 1994)

In three-level atoms where one level is the ground state and one is a metastable state, even low-intensity resonance radiation can lead to bleaching. This effect causes the radiation trapping to become nonlinear and thus greatly complicates the simulation of such a system. We set up equations to model an optically excited three-level atomic vapor in a two- or three-dimensional cylindrical cell; the model includes the effects of radiation trapping, particle diffusion, and quenching. We then develop a fast and efficient approximate method for the solution of these equations. Results are compared to Monte Carlo simulations; agreement within 15% is achieved.

PACS number(s): 32.70.Jz, 32.50.+d

I. INTRODUCTION

Resonance radiation is emitted by excited atoms when they decay to a lower state. If these atoms are surrounded by atoms of the same kind, e.g., in an atomic vapor, the resonance radiation can be absorbed and reemitted many times before it reaches the boundaries of the vapor cell. This effect is known as "radiation trapping" [1]. It is of great interest in atomic physics, e.g., atomic and molecular spectroscopy [2] and atomic line filters [3]. Radiation trapping has furthermore been investigated extensively in astrophysics (see, e.g., Refs. [4,5], and references therein), but for a range of parameters (high opacity, thermal excitation of atoms) that is of little interest for the laboratory situations of atomic physics.

Most of the papers on radiation trapping under laboratory conditions deal with trapping in two-level atoms, where the lower state is the ground state (see Refs. [6–11], and references therein). In such a system, photons are absorbed and reemitted at roughly the same wavelength. Nonlinearities, i.e., saturation in this case, only set in when the excited-state density becomes comparable to the ground-state density. This happens when intensities become comparable to the saturation intensity I_s. For transitions in the visible spectral region, I_s is rather high, on the order of 10 W/cm^2 [3].

In a three-level system where one energy level has a large lifetime (a metastable level), the situation is much more complicated. Such a system is of considerable interest not only from a theoretical but also from a practical point of view. Three-level atomic vapors play an important role in gas lasers and in atomic line filters [12,13]. Thallium (Tl, see Fig. 1 for a partial energy-level scheme) is a typical example.[1] An upper-state ($7s$) atom can decay either to the ground state ($6p_{1/2}$) or to the metastable state ($6p_{3/2}$), emitting a 378 nm uv or 535 nm green photon, respectively. The reabsorption rate will now depend on how many atoms are in the ground state and how many are in the metastable state. If all atoms are in the ground state, then the uv transition will be trapped, while the green transition will not be trapped and vice versa. Suppose now that we have a vapor cell where initially all Tl atoms are in the ground state and we illuminate this cell with external uv radiation (henceforth called "pump radiation"). In the beginning, the uv transition is trapped, while the green transition is not. This implies that the absorption of one pump photon will lead to the creation of a metastable atom with a probability that is higher than the green-to-uv branching ratio of 50%, because the "effective decay rate" (Einstein A coefficient times the probability of escape) is higher in the green than in the uv. The metastable atoms are very long lived—they act as a kind of storage reservoir—so that even quite low pump light power will deplete the ground level. This in turn leads to a decrease in the absorption of pump photons (since there are fewer absorbers), to decreased trapping of the uv transition, and, due to the creation of the metastable atoms, to increased trapping of the green transition. These effects result in a decreased

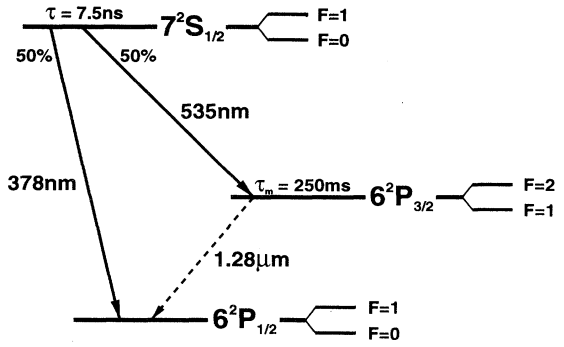

FIG. 1. Partial energy-level scheme of thallium; hyperfine splitting not to scale.

[1]As an example, in the following we specialize the discussion to Tl, but of course all considerations are equally valid for other three-level systems.

production rate of metastable atoms. The whole process is thus highly nonlinear. Due to the large lifetime of the metastable state, these "bleaching" nonlinearities (as opposed to "saturation," which implies the presence of stimulated emission) set in at an intensity that is orders of magnitude lower than that required for saturation.

To our knowledge, the trapping problem in three-level atoms has not yet been analyzed for laboratory conditions, although nonlinear trapping has been treated in the astrophysical literature. In a laboratory problem, we have to take into account many effects that are of no relevance for astrophysical computations, such as reflecting cell walls, particle diffusion, and wall quenching. Especially, the astrophysical computations are restricted to one-dimensional geometries (slabs or spheres), while we are interested in the finite cylinder geometry, which is two or three dimensional.

In our approach to the problem, we first model the relevant physical processes mathematically. We then develop an approximate method for the computation of the steady-state spatial distributions of the atoms in the three states—the upper, the metastable, and the ground state. Our method allows computations within reasonable time even for two- or three-dimensional geometries. These results are then compared to Monte Carlo simulations. A simple, closed-form equation for the average density of metastable atoms is proposed that gives a first idea on the influence of the involved parameters. As an application, we show that this method can be used to predict the absorption efficiency of a thallium atomic line filter.

II. MODELING OF THE PHYSICAL PROCESSES

Figure 2 shows the geometry of the problem. A cylindrical glass cell of length L and radius R is filled with a three-level atomic vapor, thallium in our example, and a foreign gas—a noble buffer gas is often necessary to achieve high metastable lifetime in a cell of small dimensions. The cell boundaries may be mirrored, the reflection coefficients of the mirrors can vary over the cell radius r, over the cell length z, and over the circumference angle Φ. The reflection coefficients can be different for the uv and the green. uv and green radiation is incident on the cell boundaries (top, bottom, and side walls). The incident radiation can vary with r, z, and Φ. This geometry covers most practically occurring situations. We wish to compute the steady-state distribution of the metastable and the ground-state atoms. For our computations, we make the following assumptions.

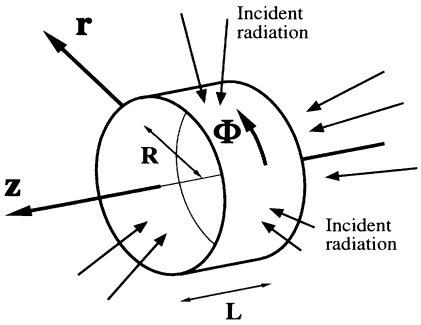

FIG. 2. Geometry of the problem.

(i) No stimulated emission occurs, i.e., the intensities are considerably below 10 W/cm^2.

(ii) The flight time of the photons is much shorter than the natural lifetime of the upper state ($7s$ in our case) atoms. For the usual excited-state lifetimes, this condition is fulfilled for cells that have dimensions of less than 1 m.

(iii) We have complete frequency redistribution in the laboratory rest frame—the frequency of the reemitted photon does not depend on the frequency of the previously absorbed photon. This is a good approximation if a buffer gas is used [14].

In a first step, we set up the steady-state rate equations for the three levels involved. For the metastable state, the density is increased by $7s$ atoms that decay to the metastable state. It is decreased (i) by the reverse process—metastable atoms absorbing green photons, (ii) by radiative decay of the metastable atoms to the ground state, (iii) by self-quenching due to Tl-Tl collisions, and (iv) by foreign-gas quenching. Furthermore, the spatial distribution of metastable atoms is changed by particle diffusion, and all metastable atoms that hit the cell walls are quenched. The resulting rate equation for the metastable atoms is

$$\begin{aligned} A^g n_{7s}(\vec{r})\, N_{\rm tot} = n_m(\vec{r}) & \\ \times N_{\rm tot} \frac{B^g}{4\pi} \int\int I^g(\vec{r},\vec{\Omega},\nu)\, C_\nu^g\, k^g(\nu)\, d\nu\, d\vec{\Omega} & \\ + n_m(\vec{r}) N_{\rm tot} \left[\frac{1}{\tau_{\rm nat}} + \frac{1}{\tau_{q,\rm Tl}} + \frac{1}{\tau_{q,\rm BG}} \right] & \\ - D\nabla^2 [n_m(\vec{r})\, N_{\rm tot}] \,, & \end{aligned} \tag{1}$$

where A^g and B^g are the Einstein coefficients for the green transition, $N_{\rm tot}$ is the Tl atomic density, n_{7s} and n_m are the fraction of Tl atoms in the $7s$ and metastable states, respectively, I^g is the intensity of the green radiation, $\vec{r}$ is the location in the cell, $\vec{\Omega}$ is the spatial angle of the direction of the radiation, ν is the radiation frequency, D is the diffusion constant of the metastable atoms through the buffer gas, and $\tau_{\rm nat}$, $\tau_{q,\rm Tl}$ and $\tau_{q,\rm BG}$ are the lifetimes of the metastable atoms due to natural decay, self-quenching, and buffer gas quenching, respectively; $k^g(\nu)$ is the absorption line shape of the green line, and

$$C_\nu^g = 1 \Big/ \int k^g(\nu)\, d\nu$$

is the line-shape normalization constant. The boundary condition for the metastable atoms is that all metastable atoms that hit the cell walls are quenched. It can be shown [15] that these absorbing boundary conditions can be approximated very well by a Cauchy-type boundary condition

$$\eta \frac{\partial n_m(\vec{r},t)}{\partial \vec{n}} \bigg|_{\vec{r}_{\rm bound}} = n_m(\vec{r}_{\rm bound}, t) \,, \tag{2}$$

where $\vec{n}$ is the normal on the cell boundary and η is 0.71 times the mean free path μ of the diffusion. The mean

free path is related to the diffusion constant by $D=\mu\bar{v}$, where $\bar{v}$ is the mean relative velocity of the colliding atoms. In most practical cases, the left-hand side of Eq. (2) is so small that we can use the Dirichlet boundary condition $n_m=0$ at the cell walls without significant error.

The density of upper-state ($7s$) atoms is decreased by spontaneous emission, and is increased by absorption of green and uv photons. The rate equation for the $7s$ atoms is thus

$$\begin{aligned}(A^g+A^{\mathrm{uv}})\,n_{7s}(\vec{r})\,N_{\mathrm{tot}} &= n_m(\vec{r})N_{\mathrm{tot}}\frac{B^g}{4\pi}\int\int I^g(\vec{r},\vec{\Omega},\nu)\,C_\nu^g\,k^g(\nu)\,d\nu\,d\vec{\Omega} \\ &+ n_{\mathrm{g.s.}}(\vec{r})N_{\mathrm{tot}}\frac{B^{\mathrm{uv}}}{4\pi}\int\int I^{\mathrm{uv}}(\vec{r},\vec{\Omega},\nu) \\ &\times C_\nu^{\mathrm{uv}}\,k^{\mathrm{uv}}(\nu)\,d\nu\,d\vec{\Omega}\,, \qquad (3)\end{aligned}$$

where superscript uv denotes parameters for the uv transition, and $n_{\mathrm{g.s.}}$ is the fraction of atoms in the ground state: $n_{\mathrm{g.s.}}\approx 1-n_m$. We can neglect energy-pooling collisions of the metastable atoms in both rate equations. The cross section for such collisions is usually much smaller than the self-quenching cross section, so that they are not a relevant loss mechanism for the metastable atoms. Furthermore, the production rate of upper-state atoms by such collisions (either directly or via some higher-lying level) is much lower than the production rate by photon absorption (note that the metastable density is related to the light intensity). Two-photon processes do not occur, since we deal with quite low light intensities.

For the thallium metastable level, the relevant parameters are a natural lifetime of 230 ms [16], self-quenching cross section $\sigma_{q,\mathrm{Tl}}=5\times10^{-16}$ cm^{-2} [17], foreign-gas quenching by argon, $\sigma_{q,\mathrm{Ar}}=5\times10^{-24}$ cm^{-2} [16], diffusion constant $D=D_0/p$, where D_0 is 0.3 cm^2 bar/s and p is the Ar pressure [16].

The equations of radiative transfer for the green and uv transitions are

$$\frac{d}{d\vec{s}}I^g(\vec{r},\vec{\Omega},\nu)=-k^g(\vec{r},\nu)\left[I^g(\vec{r},\vec{\Omega},\nu)-\frac{A^g}{B^g}\frac{n_{7s}(\vec{r})}{n_m(\vec{r})}\right], \qquad (4)$$

$$\frac{d}{d\vec{s}}I^{\mathrm{uv}}(\vec{r},\vec{\Omega},\nu)=-k^{\mathrm{uv}}(\vec{r},\nu)\left[I^{\mathrm{uv}}(\vec{r},\vec{\Omega},\nu)-\frac{A^{\mathrm{uv}}}{B^{\mathrm{uv}}}\frac{n_{7s}(\vec{r})}{1-n_m(\vec{r})}\right], \qquad (5)$$

where $d/d\vec{s}$ is the derivative in the considered direction of the radiation. As boundary conditions of the equations of radiative transfer, we have reflecting walls with reflection coefficient Γ, which can be different for uv and green radiation. We furthermore have a certain prescribed distribution I^{incident} at the cell walls. Mathematically, these boundary conditions can be formulated as

$$\begin{aligned}I^g(\vec{r}_{\mathrm{wall}},\vec{\Omega}_{\mathrm{inwards}},\nu)&=\Gamma^g I^g(\vec{r}_{\mathrm{wall}},-\vec{\Omega}_{\mathrm{inwards}},\nu) \\ &+I^{g,\mathrm{incident}}(\vec{r}_{\mathrm{wall}},\vec{\Omega}_{\mathrm{inwards}},\nu)\,, \\ I^{\mathrm{uv}}(\vec{r}_{\mathrm{wall}},\vec{\Omega}_{\mathrm{inwards}},\nu)&=\Gamma^{\mathrm{uv}} I^{\mathrm{uv}}(\vec{r}_{\mathrm{wall}},-\vec{\Omega}_{\mathrm{inwards}},\nu) \\ &+I^{\mathrm{uv,incident}}(\vec{r}_{\mathrm{wall}},\vec{\Omega}_{\mathrm{inwards}},\nu)\,.\end{aligned} \qquad (6)$$

Equations (1)–(6) completely describe the problem, incorporating all practically occurring physical processes.

III. APPROXIMATIONS

The most straightforward approach to solving the above system of integrodifferential equations is to spatially discretize the atomic densities, to discretize the radiation intensities in frequency, space, and angle, and then to replace all integrals by sums and all derivatives by differences. We get a huge system of algebraic equations that we have to solve. This approach is commonly used in astrophysics.

In a two-dimensional geometry, however, such an approach would lead to prohibitively large CPU-time requirements. We would have to discretize five variables (two spatial coordinates, two angular coordinates, and the frequency) instead of the three that are common in astrophysics. Even if we use only ten spatial and ten angular discretization steps for the additional two variables, the computational effort increases by a factor of $100^3=10^6$. In a three-dimensional geometry, the situation is even worse, since we have to include yet another spatial dimension. We thus have to find suitable approximations to reduce the size of the problem.

In a first step, we try to eliminate the dependence of the intensities on the considered direction. We expand the intensity I in a series of spherical harmonics

$$I(\vec{\Omega})=\sum_{n=0}^{\infty} I_n P_n(\mu)+\sum_{m=1}^{n}\left[a_n^m\cos(m\varphi)+b_n^m\sin(m\varphi)\right]\times P_n^m(\mu)\,, \qquad (7)$$

where $\mu=\cos(\theta)$, and θ and φ are the angles in a spherical coordinate system. We then assume that $I_2=a_2^1=b_2^1=0$ and also that all higher harmonics are zero [18]; this means physically that we neglect fast variations of the intensity with μ and φ. Since the reemission of resonance radiation is isotropic, we can expect that this assumption will be fulfilled quite well. With this simplification, the equation of radiative transfer becomes angle independent (Eddington approximation [18,19]). With $\int I\,d\vec{\Omega}=4\pi I_0=J$, we can then reduce Eq. (4) to

$$\begin{aligned}\tfrac{1}{3}\nabla^2[J^g(\vec{r},\nu)]&=\frac{1}{3n_m(\vec{r})}\vec{\nabla}[J^g(\vec{r},\nu)]\cdot\vec{\nabla}[n_m(\vec{r})] \\ &+[k_{\mathrm{all}}^g(\nu)\,n_m(\vec{r})]^2 \\ &\times\left[J^g(\vec{r},\nu)-4\pi\frac{A^g}{B^g}\frac{n_{7s}(\vec{r})}{n_m(\vec{r})}\right]. \qquad (8)\end{aligned}$$

We define $k_{\mathrm{all}}^g(\nu)$ so that $k(\vec{r},\nu)^g=k_{\mathrm{all}}^g(\nu)\,n_m(\vec{r})$; this defines k_{all}^g as the opacity that would occur if all atoms were in the metastable state (analogously for k^{uv}).

Hence, $k^g_{\rm all}\, n_m$ is the actual green opacity when a percentage n_m of the Tl atoms is in the metastable state. For the uv transition, Eq. (5) reduces to

$$\tfrac{1}{3}\nabla^2[J^{\rm uv}(\vec{r},\nu)]=\frac{1}{3[1-n_m(\vec{r})]}\vec{\nabla}[J^{\rm uv}(\vec{r},\nu)]\cdot\vec{\nabla}[1-n_m(\vec{r})] + \{k^{\rm uv}_{\rm all}(\nu)[1-n_m(\vec{r})]\}^2 \times\left[J^{\rm uv}(\vec{r},\nu)-4\pi\frac{A^{\rm uv}}{B^{\rm uv}}\frac{n_{7s}(\vec{r})}{1-n_m(\vec{r})}\right] . \quad (9)$$

For the boundary conditions, we now only need to know the incident flux $F_{\rm inc}$. The incident flux is defined as the power entering the cell through a unit area. Using the above simplifications for the angular distribution of the radiation, we can write it as

$$F_{\rm inc}(\vec{r},\nu)=\frac{1}{2}\left[\frac{1}{2}J(\vec{r},\nu)+\frac{1}{3k(\vec{r},\nu)}\frac{\partial J(\vec{r},\nu)}{\partial\vec{n}}\right] , \quad (10)$$

where k is $k^{\rm uv}_{\rm all}(1-n_m)$ or $k^g_{\rm all}\, n_m$ for uv and green flux, respectively. At a reflecting wall, the boundary condition is that the incident flux is the reflection coefficient times the emergent flux plus the externally incident flux. Mathematically, this means

$$J(\vec{r})=-\frac{2}{3k(\vec{r})}\frac{1+\Gamma}{1-\Gamma}\frac{\partial J(\vec{r})}{\partial\vec{n}}+4F_{\rm ext}(\vec{r}) . \quad (11)$$

In the rate equations, the integration over Ω becomes trivial, $\int I\, d\Omega = J$.

In a second step, we can eliminate the frequency dependence of the problem. We approximate the green and uv absorption line shapes by equivalent box-shaped lines so that the whole problem becomes frequency independent (single-frequency approximation, Milne approximation [20]). The equivalent opacities $\bar{k}^g$ and $\bar{k}^{\rm uv}$ are computed from

$$\exp(-\bar{k}L_m)=C_\nu\int k(\nu)\exp[-L_m k(\nu)]\,d\nu , \quad (12)$$

where

$$C_\nu=1\Big/\int k(\nu)\,d\nu$$

and L_m is a "typical length" of the geometry. In the classical approximation of Samson [21], L_m is set equal to L. This works, however, only for a very limited range of opacities, $k_0L<3$. We improve the approximation by using a kind of harmonic mean between the reabsorption length and the typical geometrical dimensions,

$$L_m^2=C_\nu\int\frac{k(\nu)\,d\nu}{L^{-2}+(2R)^{-2}+[0.18k(\nu)]^2} . \quad (13)$$

As we showed in Ref. [11] for the slab case, this approximation gives good results for center-of-line opacities up to $k_0L=20$. The width of the box-shaped line can be computed from the Ladenburg relation [1]

$$\Delta\nu=\frac{\lambda_0^2}{8\pi}\frac{g_u}{g_l}A\frac{N_l}{k} , \quad (14)$$

where g_u and g_l are the statistical weights of the upper and the lower levels. We now have to solve Eqs. (8)–(11) only for a single frequency. In the rate equations, the integration over frequency becomes trivial.

In our context, the Milne approximation poses some special difficulties which have not been addressed previously. First, it implicitly assumes that the incident (pump) radiation has the same line shape as the absorption line shape of the Tl vapor. This rarely is the case; even if the pump radiation comes from a thallium spectral lamp, its line shape will usually be distorted by self-absorption and thus differ considerably from the absorption line shape. We thus propose to multiply the (frequency-integrated) incident flux by a "power-adjustment" factor p_r

$$p_r^{\rm uv}=\frac{\int\{1-\exp[-k^{\rm uv}(\nu)L_m]\}k^l(\nu)d\nu\Big/\int k^l(\nu)d\nu}{\int\{1-\exp[-k^{\rm uv}(\nu)L_m]\}k^{\rm uv}(\nu)d\nu\Big/\int k^{\rm uv}(\nu)d\nu} , \quad (15)$$

where $k^l(\nu)$ is the line shape emitted by the uv pump lamp (and analogously for incident green radiation). This factor is a measure of the "overlap" between the spectral shapes of the incident radiation and the absorption line shape in the vapor cell. It becomes unity when the shapes are identical. Multiplying the incident flux with p_r, we get the correct pump absorption within one "typical" distance L_m. However, we cannot get the correct *spatial* distribution of the points of absorption. If p_r is very small (e.g., if the incident radiation comes from a white light source, or, even worse, from a strongly self-reversed spectral lamp), we can anticipate that the points of absorption in the Milne approximation will be concentrated too much near the side walls. This is a basic problem of using a single-frequency approximation (box-shaped line)—it intrinsically neglects the photons in the wings of the spectral line, i.e., photons emitted at such frequencies ν that $k_0k(\nu)R$ is much smaller than the line-center opacity. These photons can penetrate much farther into the cell than center-of-line photons.

In our derivation, we used the assumption "if $k^g_{\rm all}$ is the green opacity for the case that all atoms are in the metastable state, then $k^g_{\rm all}\, n_m$ is the actual opacity when a percentage n_m of the Tl atoms is in the metastable state" (and analogously for $k^{\rm all}_{\rm uv}$). This assumption is strictly valid only for the frequency dependent opacity $k(\nu)$. Since the relation between the Tl density (center-of-line opacity) and the equivalent opacity is nonlinear, it is not true for the equivalent opacities $\bar{k}$. We circumvent this problem by computing $\bar{k}$ in each step of the iteration anew as

$$\bar{k}^g_{\rm all}=\frac{\bar{k}^g_1}{\bar{n}_m} , \quad (16)$$

where $\bar{n}_m$ is n_m averaged over the cell and $\bar{k}^g_1$ is computed from Eq. (12) with $k(\nu)=k^g_{\rm all}(\nu)\bar{n}$. Strictly speaking, this also works only for a *homogeneous* distribution of metastable atoms; however, the error introduced by ignoring the inhomogeneities in the definition of the equivalent opacity is very small. Finally, it must be em-

phasized that the single-frequency approximation gives good results only for opacities smaller than 3 (for the classical Milne theory) and 20 (for our improved version), respectively.

Using a single-frequency approximation means that the computational effort is reduced by a factor equal to the number of frequency discretization points. This number usually has to be on the order of 30–100. Hence the single-frequency approximation is a noteworthy saving. The error in $\bar{n}_m$ is smaller than about 10% for the range of parameters we are interested in (center-of-line opacity $k_0 L < 20$); this is better than the accuracy of the available atomic data and thus amply sufficient.

IV. COMPUTATIONAL ASPECTS

The simplified rate equations and equations of radiative transfer are a coupled system of integrodifferential equations with Cauchy boundary conditions. As mentioned in the Introduction, the whole problem is highly nonlinear. However, we can deal with that nonlinearity by a simple iteration procedure. If we assume that n_m and n_{7s} are known, then the simplified equations of radiative transfer, Eqs. (8) and (9), are second-order *linear* differential equations with nonconstant coefficients; we solved them by a finite-differences (FD) algorithm to get the green and uv intensities. If these intensities are known, the rate equations are linear differential equations for n_{7s} and n_m, which are also solved with finite differences. These solutions for the densities are then used for the next solution of the equations of radiative transfer. Three or four iteration steps are usually sufficient to get convergence (the difference between the iteration steps becomes smaller than 1%).

In order for the iteration to converge rapidly, the first guesses for n_m and n_{7s} should be close to the actual value. We can usually make a reasonable guess about $\bar{n}_m$, the fraction of atoms that are in the metastable state, averaged over the cell (see below). On the other hand, it is practically impossible to give generally valid guesses for the *shape* of the distribution of the metastable atoms. It is thus reasonable to assume for the first guess that the metastable atoms are homogeneously distributed in the cell; only at the cell walls we have $n_m = 0$ according to the boundary conditions. We thus recommend to use for the first iteration the distribution

$$n_m = \left[1 + \frac{2(1+\bar{k}^g_{\text{all}} L^g_m) h\nu N_{\text{tot}} R^2 \pi L}{F^{\text{abs}}_{\text{all}} \tau} \right]^{-1}, \tag{17}$$

where

$$F^{\text{abs}}_{\text{all}} = \frac{F^l}{(L^{-2}+R^{-2})^{1/2}} \frac{\int k^l(x) k^{\text{uv}}(x) dx}{\int k^l(x) dx} \tag{18}$$

everywhere except at the cell boundaries ($n_m = 0$); for n_{7s} we recommend $n_{7s} = n_m / A\tau$. A bad initial guess will usually lead to about two or three additional iterations, i.e., it will about double the CPU time. These equations also give a first estimate on the influence of the various parameters on the average densities.

Nonequidistant discretization for the finite-difference computations is essential for efficient calculations. If we have low particle densities and low buffer gas pressures, the distribution of the metastable atoms will be quite similar to the lowest-order diffusion mode, so it drops slowly from its maximum value near the center of the cell to 0 at the cell walls. In that case, the choice of the discretization does not matter very much. If, on the other hand, the buffer gas pressure is large, n_m has quite large values at all points except close to the cell boundary, where it rapidly drops from large values to 0. In this region, we need a quite fine discretization. If we chose equidistant discretization, the computational effort would increase like $1/h^6$, where h is the distance between two discretization points.

The use of our method allows the computation of a problem which copes not only with nonlinearities but also with two- or three-dimensional geometries within reasonable computer time. On a VAX-Alpha 4000, computations take about 5 sec (with 150 spatial discretization points). With a standard IBM-PC (486/66 MHz), computation times are estimated to be a factor 15 longer. These values are typical for two-dimensional geometries, e.g., a finite cylinder that is independent of angle. Such a situation is of great practical interest, and the examples in Secs. V and VI use such a geometry. However, our algorithm is also valid for three-dimensional geometries.

V. COMPARISON WITH MONTE CARLO SIMULATIONS

The algorithm described above contains approximations to the angular and to the frequency distribution of the radiation. In order to check the errors introduced by these approximations, we compare the results of our FD algorithm to a quite different approach, a Monte Carlo (MC) simulation [22]. In the MC simulation, we trace a photon on its way through the vapor. Parameters such as frequency, point of absorption, direction of reemission, etc., are chosen at random from the appropriate statistical distributions. Since the distribution of absorbers is inhomogeneous, we have to compute the absorption coefficient for each path separately. The vapor cell is divided into many subcells. We assume that the metastable density is constant within each subcell. The opacity "seen" by a photon along a certain direction will of course vary from subcell to subcell. We thus have to compute the intersections of the photon path with the subcell boundaries and to add up the opacities of the path lengths within each subcell. If a uv photon is absorbed and a green photon is reemitted, this means that the absorbing-reemitting atom has been transferred from the ground state to the metastable state (and vice versa); the metastable population of the appropriate subcell is then increased by 1. As there are many photons and atoms (typically in the order of 10^{12}), we introduce a "reduction factor" ρ (e.g., $\rho = 10^9$) by which we divide the number of emitted photons and the number of atoms in the vapor cell.

We also have to include the effects of particle diffusion and quenching. After observing the vapor for a time τ_{step}

[i.e., after the lamp has emitted $P^l \tau_{step}/(\rho h\nu)$ photons, where P^l is the power emitted by the lamp], we compute the effect of diffusion and quenching for the distribution of metastable atoms within the time τ_{step}. We chose an analytical computation of metastable decay, because an MC simulation of the diffusion of metastable atoms through the buffer gas would take too much CPU time—each metastable state undergoes typically 10^8 collisions with the buffer gas during one lifetime. τ_{step} must be chosen small enough that the vapor does not change appreciably during that time interval. On the other hand, τ_{step} must not be chosen too small, or roundoff errors could become a problem. $\tau_{step} \approx 0.05 \tau_{metastable}$ has turned out to be a good compromise.

In the MC simulation, simplifications that are necessary for the FD computations can be lifted and, in addition, the temporal development of the metastable population can be observed. Furthermore, MC results can be made very accurate by choosing a sufficiently small reduction factor ρ, albeit at the cost of large CPU-time requirements.

As an example for the good agreement between MC and FD results, we consider the case of a cylindrical Tl vapor cell where uv radiation is incident on the cell side walls. The incident uv radiation comes from a toroidally shaped thallium spectral lamp. Such a situation is of practical interest for the design of atomic line filters (see also Sec. VI).

We use the following set of parameters: cell radius=2.5 cm, cell length=1.5 cm, buffer gas argon, single-isotope ^{205}Tl in the cell. The top of the cell is mirrored for all wavelengths. The uv (pump) lamp has a center-of-line opacity $k_0 R = 15$, and we assume a parabolic spatial distribution of $7s$ atoms over the lamp radius; the lamp contains a natural mix of Tl isotopes and 10 mbar argon. For the FD computations, we approximate the pump lamp by an equivalent area source (i.e., a circular band at $r = R_{torus}$, where R_{torus} is the radius of the torus of the pump lamp). The angular distribution of the emergent radiation is assumed to be Lambertian. The line shape of the emergent radiation is self-reversed; it is determined by the line-center opacity and the distribution of the $7s$ atoms in the pump lamp.

There are mainly three parameters in the rate equation and in the transfer equation that can vary over a wide range: the particle density N_{tot}, the diffusion constant D (which in turn depends on the buffer gas pressure), and the incident flux (which is determined by the pump lamp power). In the following three figures, we vary these three parameters. We compare the mean percentage of metastable atoms as computed by the FD and the MC method in order to assess the errors introduced by the underlying assumptions and approximations of the FD method. Figure 3 shows $\bar{n}_m$ as a function of the Tl density, varying over two orders of magnitude (10^{11}–10^{13} cm^{-3}) for 80 mbar buffer gas pressure. The agreement between MC and FD is always better than 12%. Figure 4 shows the average percentage of metastable atoms in the cell as a function of the buffer gas pressure. We again see excellent agreement between FD and MC results. Increasing the buffer gas pressure increases $\bar{n}_m$, because it

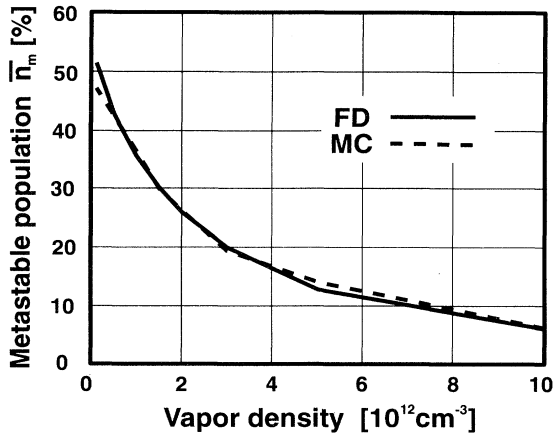

FIG. 3. Percentage of thallium atoms in the metastable state averaged over the cell, $\bar{n}_m$, as a function of the vapor density: FD computations (solid) and MC simulations (dashed). The vapor cell is filled with single-isotope Tl and 80 mbar Ar. Pump lamp power is 40 mW.

increases both the lifetime of the metastable atoms (at least up to $p = 500$ mbar, where buffer gas quenching becomes dominant) and the power-adjustment factor p_r—the absorption line becomes broader, so that more pump photons can be absorbed. Figure 5 finally shows n_m as a function of the pump lamp power (for $N_{tot} = 10^{11}$ cm^{-3} and 250 mbar argon pressure); we see that population inversion (i.e., $\bar{n}_m > 2/3$) can be achieved with only 60 mW pump lamp power. Baranov [23] proposed to construct a laser at 1.28 μm by using the population inversion in a thallium vapor and also experimentally demonstrated the feasibility of such a population inversion.

We see that the results of FD and MC computations agree within 15%, as we varied the particle density, the diffusion constant, and the light intensities over orders of

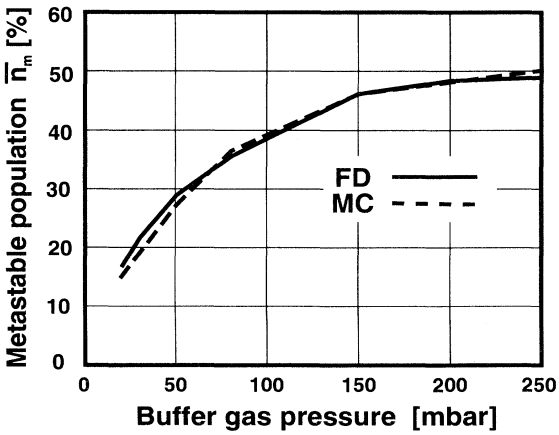

FIG. 4. Percentage of Tl atoms in the metastable state averaged over the cell, $\bar{n}_m$, as a function of the argon pressure: FD computations (solid) and MC simulations (dashed). Tl density in the cell is 10^{12} cm^{-3}. Pump lamp power is 40 mW.

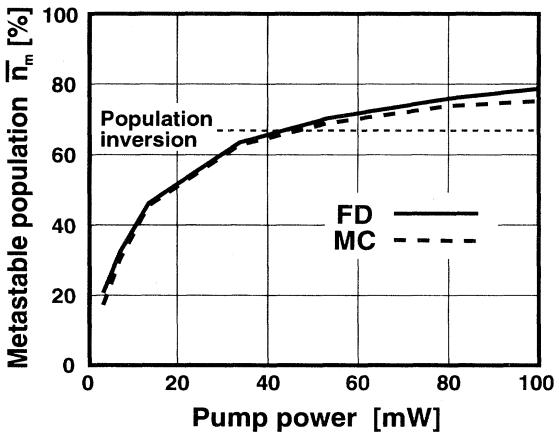

FIG. 5. Percentage of Tl atoms that are in the metastable state averaged over the cell, $\bar{n}_m$, as a function of the pump lamp power: FD computations (solid) and MC simulations (dashed). Tl density in the cell is 0.3×10^{12} cm^{-3}, argon pressure is 250 mbar.

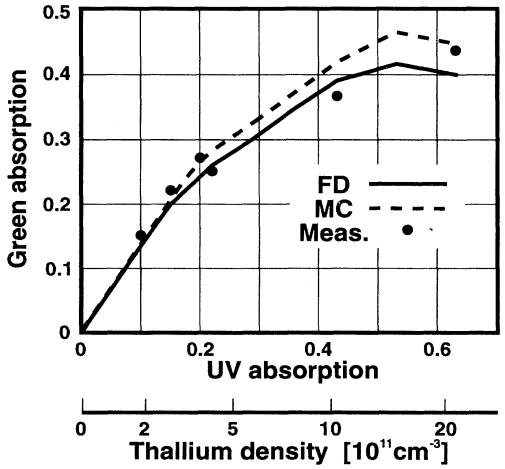

FIG. 6. Absorption of the green probe light beam (which is proportional to the metastable Tl density along the cell axis) as a function of the absorption of a uv probe light (which is proportional to the total Tl density along the cell axis): FD computations (solid), MC simulations (dashed) and measurements (dots). The vapor cell is filled with single-isotope Tl and 80 mbar Ar.

magnitude, and all this with the most problematic pump line shape (a strongly self-reversed line shape, see Sec. III). This shows that our method is a very robust algorithm.

VI. APPLICATION

One application of an optically pumped three-level atomic vapor lies in atomic line filters [12,13]. Such a filter consists of a quartz cell filled with an atomic vapor, and two dyed-glass filters. In the vapor cell, signal radiation is absorbed on one atomic transition and reemitted at another. The two dyed-glass filters are used to eliminate all radiation that is not wavelength converted by this absorption-reemission process. In the thallium atomic line filter, green signal radiation is absorbed by metastable thallium atoms and reemitted in the uv on the $7s-6p_{1/2}$ transition. For an efficient filter, it is necessary to have a large number of metastable atoms in the cell. These metastable atoms are produced by activating the filter shortly before use by sending uv pump radiation from a spectral lamp into the vapor cell. This transfers atoms from the $6p_{1/2}$ ground state via the $7s$ state to the metastable $6p_{3/2}$ state.

We measured the absorption of green probe radiation in such a filter as a function of the Tl density (i.e., by variation of the temperature). Green absorption is a measure of the density of metastable atoms along the axis of the vapor cell. The Tl density was determined by measuring the uv absorption of the unpumped vapor; this gives more reliable results than a temperature measurement and computing N_{tot} from the vapor pressure curves. The parameters of the vapor cell and of the pump lamp were the same as those we used in Sec. V. The argon pressure was 80 mbar, and the pump lamp power was 40 mW.

We simulated the experiment with both the FD and the MC method and determined the metastable density as a function of the particle density. From this, we can easily compute the green absorption as a function of the uv absorption. Figure 6 compares the simulation results to the experimental results. We see that the agreement between FD computations, MC simulations, and the measurements is excellent. The difference always stays below 15%. Thus our model allows a good prediction of the actual behavior of an atomic line filter. The high efficiency of our FD method makes it a useful simulation tool for the optimization of such filters.

VII. SUMMARY AND CONCLUSION

We modeled the behavior of a three-level atomic vapor in a cylindrical cell, including the effects of nonlinear radiation trapping, arbitrary line shape of the incident radiation, foreign gas quenching, finite geometry, particle diffusion, and reflecting cell walls. We presented a fast approximate method for the evaluation of the appropriate equations. The results were compared to Monte Carlo simulations and agreement within 15% was achieved.

ACKNOWLEDGMENTS

This work was done for the European Space Agency under ESTEC Contract No. 9516/91/NL/PB(SC). We thank the Jubiläumsfonds der Gemeinde Wien for additional financial support.

[1] A. G. Mitchell and M. W. Zemansky, *Resonance Radiation and Excited Atoms* (Cambridge University Press, Cambridge, England, 1961).
[2] A. Corney, *Atomic and Laser Spectroscopy* (Oxford University Press, Oxford, 1977).
[3] J. A. Gelbwachs, IEEE J. Quantum Electron. **24**, 1266 (1988).
[4] D. Mihalas, *Stellar Atmospheres,* 2nd ed. (Freeman, San Francisco, 1978).
[5] C. J. Cannon, *Transfer of Spectral Line Radiation* (Cambridge University Press, Cambridge, England, 1986).
[6] T. Holstein, Phys. Rev. **72**, 1212 (1947).
[7] L. M. Biberman, Zh. Eksp. Teor. Fiz. **17**, 416 (1947) [Sov. Phys. JETP **19**, 584 (1949)].
[8] C. van Trigt, Phys. Rev. **181**, 97 (1969).
[9] A. V. Phelps, Phys. Rev. **110**, 1362 (1958).
[10] F. E. Irons, J. Quant. Spectrosc. Radiat. Transfer **22**, 1 (1979).
[11] A. F. Molisch, B. P. Oehry, and G. Magerl, J. Quant. Spectrosc. Radiat. Transfer **48**, 377 (1992).
[12] B. P. Oehry, W. Schupita, and G. Magerl, Opt. Lett. **16**, 1620 (1991).
[13] B. P. Oehry, W. Schupita, B. Sumetsberger, A. F. Molisch, and G. Magerl, in *Lidar Techniques for Remote Sensing,* edited by Ch. Werner, SPIE Proc. Vol. 2310 (SPIE, Bellingham, WA, 1994), p. 51.
[14] T. M. Colbert and B. Wexler, Phys. Rev. A **47**, 2156 (1993).
[15] P. M. Morse and H. Feshbach, *Methods of Theoretical Physics* (McGraw-Hill, New York, 1953).
[16] E. B. Aleksandrov, A. V. Baranov, and V. N. Kulyasov, Opt. Spektrosk. **44**, 1065 (1978) [Opt. Spectrosc. (USSR) **44**, 624 (1978)].
[17] R. C. Pickett and R. Anderson, J. Quant. Spectrosc. Radiat. Transfer **9**, 697 (1969).
[18] R. G. Giovanelli, Aust. J. Phys. **12**, 164 (1959).
[19] R. G. Giovanelli, in *Progress in Modern Optics,* edited by E. Wolf (North-Holland, Amsterdam, 1963).
[20] E. A. Milne, J. London Math. Soc. **1**, 40 (1926).
[21] E. W. Samson, Phys. Rev. **40**, 940 (1932).
[22] A. F. Molisch, W. Schupita, B. P. Oehry, B. Sumetsberger, and G. Magerl, in *Proceedings 5th European Quantum Electronics Conference, Amsterdam, 1994* (IEEE, Piscataway, 1994), p. 251.
[23] A. V. Baranov, Opt. Spektrosk. **46**, 617 (1979) [Opt. Spectrosc. (USSR) **46**, 347 (1979)].